

Article

Comparative Analysis of a New Class of Symmetric and Asymmetric Supercapacitors Constructed on the Basis of ITO Collectors

Michał Gocki ¹, Agnieszka Jakubowska-Ciszek ²  and Piotr Pruski ^{2,*} 

¹ Scientific and Didactic Laboratory of Nanotechnology and Material Technologies, Faculty of Mechanics and Technology, Silesian University of Technology, 44-100 Gliwice, Poland

² Faculty of Electrical Engineering, Silesian University of Technology, 44-100 Gliwice, Poland

* Correspondence: piotr.pruski@polsl.pl

Abstract: The paper presents the results of research on new electroconductive polymer materials, based on polypyrrole, for the different supercapacitor constructions, i.e., the symmetric and asymmetric constructions. All the supercapacitors considered contain ITO collectors. Measurements of the complex impedance frequency characteristics were performed for these elements using the electrochemical impedance spectroscopy (EIS) method. Selected fractional-order models, known from the literature, have been used to model the impedance of these elements. The Particle Swarm Optimization (PSO) algorithm was used to estimate the model parameters. Selected estimation results, their comparison, and conclusions are also presented in the paper. The type of active electrolyte component has the greatest impact on the shape of the impedance frequency characteristics. In most cases, the highest capacitance values and the smallest resistance values were obtained for asymmetric supercapacitors.

Keywords: symmetric and asymmetric supercapacitors; fractional-order impedance; model parameters estimation; ITO collectors



Citation: Gocki, M.; Jakubowska-Ciszek, A.; Pruski, P. Comparative Analysis of a New Class of Symmetric and Asymmetric Supercapacitors Constructed on the Basis of ITO Collectors. *Energies* **2023**, *16*, 306. <https://doi.org/10.3390/en16010306>

Academic Editors: Carlos Miguel Costa and Fangming Jiang

Received: 14 November 2022

Revised: 11 December 2022

Accepted: 26 December 2022

Published: 27 December 2022



Copyright: © 2022 by the authors. Licensee MDPI, Basel, Switzerland. This article is an open access article distributed under the terms and conditions of the Creative Commons Attribution (CC BY) license (<https://creativecommons.org/licenses/by/4.0/>).

1. Introduction

1.1. Context of the Study and Related Works

Electrochemical double layer capacitors (EDLCs), which are also called supercapacitors, are gaining more and more interest, among others, in the transportation industry [1–3], renewable energy systems [4,5], and emergency power systems [6], which are used during a power failure in important ICT (Information and Communication Technologies) facilities. Their positive aspects such as high power density, long life cycle, and low-voltage operation make them attractive devices for this industry sector. High-power density systems are used in recuperative braking systems in electric vehicles. They were originally used in traction units, but with the development of electromobility, they have also been used in electric cars and buses. The main limitation of electric double layer capacitors is their low energy density. The solution to this problem is the use of supercapacitors and batteries in a single system [7]. In such a system, capacitors ensure high power density, whereas batteries are responsible for high energy density. In addition, supercapacitors can be used as small flexible energy sources for clothing. Supercapacitors used in wearable applications have electrodes made of metal oxides and carbon material [8–10].

Polypyrrole is characterized by good electrochemical properties and therefore it is used as an electrode material for supercapacitors. This type of electrically conductive polymer is also used in composite materials with carbon materials and inorganic oxides. A research team from Shanghai Jiao Tong University has developed supercapacitors with electrodes made of manganese oxide (IV) and polypyrrole composite materials. The materials were synthesized through a chemical reaction. Devices containing the mentioned materials had

a good specific capacitance of 50 F/g. These results indicate that MnO₂/PPy composites with regular core-shell structures could be used to build supercapacitor electrodes with good electrochemical parameters [11].

Composite materials of polypyrrole and inorganic compounds such as titanium carbides (Ti₃C₂T_x) are also used in supercapacitors. Researchers from Wuhan University of Technology have developed supercapacitors containing polypyrrole and titanium carbide electrodes. In the tests, polypyrrole was deposited by electropolymerization on titanium carbide films. Devices with such electrodes have a specific capacity of up to 420 F/g [12].

Electrochemical devices can also be used as part of our clothes. Researchers from Hong Kong Polytechnic University have developed a wearable supercapacitor in the form of a fiber. Such a one-dimensional device can be woven or sewn into another material and store energy. Such stored energy could power the heating elements of a jacket or T-shirt. Such a thread was developed on the basis of a nickel/cobalt composite and a polypyrrole composite. The polypyrrole acted as the negative electrode, while the metal composite acted as the positive electrode. Asymmetric solid-state supercapacitors (ASCs) demonstrated high electrochemical properties and excellent mechanical flexibility under various degrees of deformation. The highest volumetric capacity was 14.69 F/cm³ [13].

1.2. Research Gap

Traditional supercapacitors are based on an electrical double Helmholtz layer. The Helmholtz layer is formed at the interface between the electrolyte and the electrode. In the construction of this type of device, electrodes are materials with a large internal surface. The need to use such material solutions results from the physicochemical dependence, which means that the increase in the capacity of the device is directly proportional to the increase in the surface area of the electrodes. Polymer supercapacitors are a special group of devices that are characterized by an energy storage mechanism slightly different from traditional dielectric capacitors. These types of devices have two energy storage mechanisms: a double Helmholtz layer and reduction and oxidation reactions of conductive polymers. The energy in this case is generated during the charge transfer that occurs in the redox reaction. When active materials are selected as necessary for the implementation of the device, particular attention should be paid to substances capable of producing surface reduction and oxidation reactions. Materials showing such properties are conductive polymers [10,14–16].

ITO plates are characterized by good electrical conductivity; such properties are provided by the conductive layer of tin oxide and indium oxide. This material is characterized by high light transmittance and is colorless. For this reason, it is used in optoelectronics. This substrate is well suited for the deposition of electrically conductive materials, such as conductive polymers and inorganic oxides. It is possible to deposit strictly ordered ZnO crystal structures of the wurcite type on ITO plates [17].

Measurement methods for energy storage devices can be divided into two types: constant current [18] and alternating current methods [19]. During measurements with constant current methods, there are strong disturbances caused by polarization phenomena. Resistance measurements with these methods are overestimated, and with low-voltage measurements, current flow is blocked when blocking electrodes are used. The cognitive importance of such measurements is insignificant. The second type of measurements is alternating current methods, including electrochemical impedance spectroscopy (EIS). The discussed measurement method allows high precision during measurements and is often used to assess heterogeneous charge transfer parameters and study the two-layer structure. This technique has applications in battery research, fuel cell development, sensors, corrosion, and physical electrochemistry, and can also provide information on reaction parameters, corrosion rate, electrode surface porosity, coating properties, mass transport, and interfacial capacitance measurements. It is used in many fields of science, such as chemistry, materials engineering, electrical engineering, and electronics [7–9,19,20].

The frequency characteristics of the impedance, as well as the time response waveforms of currents and voltages, show that there is a difference between the models of classic dielectric capacitors and supercapacitors (EDLC capacitors) [21,22]. Scientists and electrical engineers noticed that their behavior can be described by fractional differential-integral calculus [1,23]. In the frequency domain, a few representative impedance models have been developed, from simple fractional-order model, to models based on fractional poles and zeros, to electrochemical impedance models derived from electrochemical impedance spectroscopy (EIS) measurements [24–27]. The models discussed will be presented, described, and compared in the next sections of the paper.

1.3. Motivation and Contribution

The aim of the paper is to estimate the fractional-order model parameters of the examined supercapacitors with ITO collectors and to compare their properties for various electrode materials and active electrolyte components.

The optimization method used to estimate the parameters of the supercapacitor models is based on the approximation of the measurement characteristics of a modulus $|Z(f)|$ and an argument $\varphi(f)$ of the impedance, with the characteristics calculated from the equation of the selected fractional-order models.

The original authors' contribution is as follows:

1. Construction of tested supercapacitors with a unique combination of active materials; the unique design results from proper selection of electrode materials and electrolyte active ingredients;
2. Development of a method for selecting search ranges of the parameters of supercapacitor models and a method of normalization of the measured characteristics;
3. Selection of models known in the literature that best approximate the characteristics of the supercapacitors studied, verification of the parameters of selected fractional-order models, and evaluation of the quality of their matching to the examined elements.

2. Materials and Methods

2.1. Materials Used for Symmetric and Asymmetric Supercapacitors

In the research, symmetric and asymmetric supercapacitors were constructed. Symmetric arrays have the same electrode material on each of the two collectors, while asymmetric arrays have two different types of electrode materials. In addition, the systems were differentiated by four types of electrolytes, in which different active salts were used. The tested supercapacitors were made on ITO plates. Electropolymerization of pyrrole and 3-n-octylpyrrole was performed by cyclic voltammetry using a CHI 660 potentiostat and a three-electrode system. Polymers were applied to the surfaces of the plates. The weight of the polymer on both collectors is approx. 35 μg (micrograms) in each device. The distance between the two collectors containing the polymer is approximately 70 μm [20].

The pyrrole molecule undergoes an electropolymerization reaction according to a standard mechanism. The monomer is oxidized to a radical cation, and then, in an additional reaction step, the two oxidized pyrrole structures form a dimer that has two positive charges. The additional reaction of subsequent cation radicals proceeds to the point where the macromolecule becomes insoluble in the system and the polymer precipitation occurs. Figure 1 shows the mechanism of polypyrrole electropolymerization [28].

In the systems tested, electrolytes containing poly(methyl methacrylate) (Alfa Aesar, MW = 550,000), acetonitrile (Acros, 99%), propylene carbonate (Prosynth, 99%) and a variable active ingredient in the form of lithium and tetrabutyl salts were used. The following salts were used as active electrolyte components: lithium perchlorate (LiClO_4) (Acros, pure), tetrabutylammonium perchlorate (NBu_4ClO_4) (Fluka, 98%), tetrabutylammonium triflate ($\text{NBu}_4\text{CF}_3\text{SO}_3$) (Fluka, 98%) and lithium trifluoromethanesulfonate (LiCF_3SO_3) (Fluka, 98%).

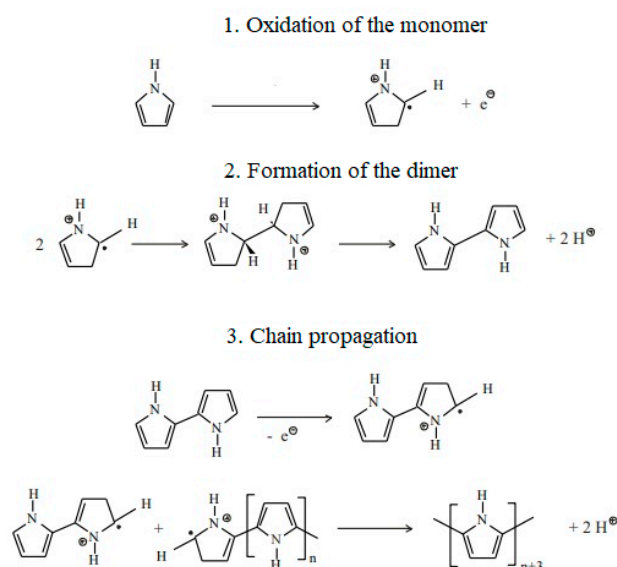


Figure 1. Mechanism of pyrrole electropolymerization [28].

The devices were tested by the EIS method using the Bio-Logic SP-150 potentiostat in the laboratory of the Department of Physicochemistry and Polymer Technology, Faculty of Chemistry, Silesian University of Technology.

Symmetric and asymmetric supercapacitors were also tested by cyclic voltammetry (CV). This technique relies on recording the working electrode's current intensity, depending on the given electrode potential. As a result of the cyclic voltammetry measurement, a voltammetric loop was obtained for each system. During polymer supercapacitors tests, the potential window in the range from -0.2 V to 0.8 V was used, because such a potential range provided the correct ranges of recorded current and, at the same time, was safe for the tested materials. The specific capacitance was calculated using an equation [29]:

$$C_p = \frac{A}{2 \cdot m \cdot \mu \cdot (V_2 - V_1)}, \quad (1)$$

where: C_p —supercapacitor specific capacitance, F/g, A —voltammogram loop area, $A \cdot V$, m —mass of the electrode substance, g, μ —system scanning speed, V/s , $V_2 - V_1$ —potential window value, V.

2.2. Fractional-Order Supercapacitor Models in Frequency Domain

Based on many scientific studies conducted on supercapacitors, it can be seen that both the frequency characteristics and the waveforms in the systems containing them differ from the characteristics and waveforms occurring in circuits with classic dielectric capacitors [21,22]. This is due to their features, such as high capacity (up to several thousand farads), electrochemical structure, and relatively large series internal resistance (ESR) [1,23]. This is the reason why fractional differential calculus is increasingly being used to describe their behavior [24–27]. In [24–26], the values of the fractional-order model parameters were obtained for selected commercial supercapacitors. At the same time, research is ongoing on new realizations of fractional-order capacitors [30].

The simplest fractional-order impedance model of a supercapacitor is given by a relation [22]:

$$Z_C(j\omega) = R_C + \frac{1}{(j\omega C_\alpha)^\alpha}, \quad (2)$$

where: R_C —series equivalent resistance (ESR) of the supercapacitor, C_α —pseudocapacitance, α —fractional-order parameter (dimensionless). The parameter C_α is called a pseudocapacitance, because its unit is not Farad, as in classic dielectric capacitors, but $F/s^{(1-\alpha)}$.

The advantage of the above model is its simplicity, but the main disadvantage is a very limited frequency range (up to 50–250 mHz), where the model is accurate [22].

Therefore, several more complicated, but at the same time more accurate, supercapacitor models in the frequency domain have been developed, on the basis of electrochemical impedance spectroscopy (EIS) measurements. In the research described in the paper, models applicable for a wide range of frequencies were taken into account.

An example of such models is the model based on poles and zeros of the fractional-order impedance, described as [24]:

$$Z_C(j\omega) = R_C + k \frac{\left(1 + j\frac{\omega}{\omega_0}\right)^\alpha}{(j\omega)^\beta}, \quad (3)$$

where: R_C —series equivalent resistance (ESR) of the supercapacitor, ω_0 —limiting pulsation, k —parameter related to the reciprocal of the capacitance (elastance) of the supercapacitor, α, β —fractional parameters (dimensionless).

Individual parameters of the model (2)— $R_C, \omega_0, \alpha, \beta$ and k —can be determined with good accuracy from the Nyquist and Bode frequency characteristics.

Using the EIS method, more complex models of fractional-order supercapacitors were also derived. They describe single electrochemical structures that correspond to the phenomena that occur in supercapacitors in different frequency ranges [24–27]. Several elements were introduced in these models, the transfer functions of which are described by the following relations [24]:

- Warburg impedance:

$$W(j\omega) = \frac{Z_0}{\sqrt{j\omega}}, \quad (4)$$

- Warburg limited impedance:

$$O(j\omega) = \frac{Z_0 \coth(B\sqrt{j\omega})}{\sqrt{j\omega}}, \quad (5)$$

- Havriliak–Negami function:

$$H(j\omega) = \frac{1}{j\omega(C_0 - C_\infty)[1 + (j\omega\tau)^\mu]^\Phi}, \quad (6)$$

where: Z_0, B —parameters; C_0, C_∞ —supercapacitor's capacitance at low ($f \rightarrow 0$) and high frequencies ($f \rightarrow \infty$); τ —parameter related to operating temperature; μ, Φ —fractional-order parameters.

Warburg impedance represents linear diffusion in a semi-infinite space, dependent on the frequency and the interference potential. The constrained Warburg element describes a linear diffusion in a uniform layer of limited thickness [24–26]. Examples of fractional-order topologies using the Warburg impedance and the Warburg limited impedance, with four or five parameters, respectively, are shown in Figure 2.

The Havriliak–Negami function is a part of the most universal supercapacitor model in the frequency domain. The supercapacitor model taking into account five parameters (L, R_1, R_2, R_3, C) and the five-parameter H function are presented in Figure 3. It is the most accurate description of a real supercapacitor in a wide range of frequencies.

Work is also being conducted on new models of fractional-order supercapacitors, including the development of a model that combines part of the integer order of the supercapacitor capacitance and parts of the fractional order, which together would describe all the phenomena occurring inside the supercapacitor [23,26,27].

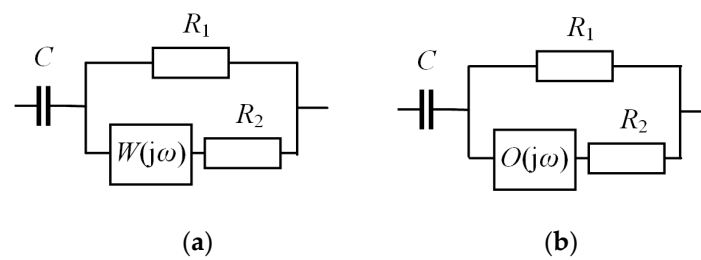


Figure 2. Topologies of fractional-order supercapacitor models: (a) four-parameter structure with Warburg impedance, (b) five-parameter structure with limited Warburg impedance.

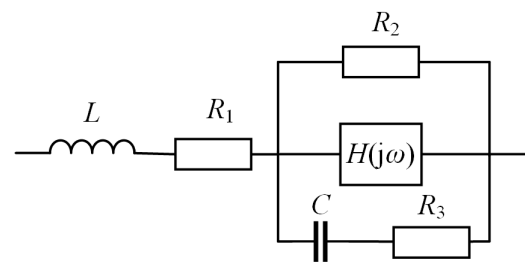


Figure 3. Fractional-order supercapacitor topology using the Havriliak–Negami function.

A separate issue is the identification of the parameters of the individual supercapacitor models. Various identification methods have been developed using, for example, the resonance phenomenon in a series circuit [31]. However, in the case of obtaining Nyquist or Bode spectra, a good solution is to estimate the model parameters using optimization methods and algorithms.

2.3. The Method of Estimation of the Model Parameters

The method of estimation of the parameters of the supercapacitors models used in the article consists of the approximation of the measurement characteristics of a modulus $|Z(f)|$ and an argument $\varphi(f)$ of the impedance, with the characteristics calculated based on the equation of the selected model [32].

Before the estimation of model parameters, the initial indicative values of these parameters are calculated. The parameters related to the resistance are taken equal to the real parts of the supercapacitor impedance for the highest frequency, because the capacitive reactance decreases as the frequency increases, while the factor associated with, for example, the series resistance ESR, remains. The parameters related to the capacitance are calculated on the basis of an imaginary part of the impedance for the lowest frequency, for which the capacitive reactance is the highest. The ranges of the search for individual model parameters are selected experimentally to obtain satisfactory approximation accuracy, taking into account the physical sense of these parameters, the physical and electrochemical phenomena occurring in the supercapacitors.

The characteristic approximation consists of a minimization of an objective function defined as a mean square error between the measurement and the approximating characteristics. A normalization of the measurement and approximating characteristics was used to obtain similar orders of magnitude of their values [32]:

$$|\tilde{Z}|(f) = \frac{|Z|(f)}{\max_f(|Z|(f))}, \quad \tilde{\varphi}(f) = \frac{\varphi(f)}{\max_f(|\varphi|(f))}, \quad (7)$$

where, as reference values for measurement and approximating characteristics, the maximum values of appropriate measurement characteristics were used, which do not change in the approximation process.

The objective function ε is therefore the form [32]:

$$\varepsilon(\mathbf{K}) = \sum_{i=1}^n \left(\left| \tilde{Z} \Big|_m (f_i) - \left| \tilde{Z} \Big|_a (f_i, \mathbf{K}) \right. \right)^2 + \sum_{i=1}^n (\tilde{\varphi}_m(f_i) - \tilde{\varphi}_a(f_i, \mathbf{K}))^2, \quad (8)$$

where: \mathbf{K} —vector of the searched parameters of the model, i —number of a point of frequency characteristic, n —number of points of frequency characteristic, the same for $|Z(f)|$ and $\varphi(f)$, where index ‘m’ means measurement characteristic and index ‘a’—approximating characteristic, calculated based on the searched model parameters.

The Particle Swarm Optimization (PSO) algorithm [33–37] was used to minimize the objective function. It allows finding a global minimum of an objective function with satisfactory accuracy and speed, despite the large search area and the occurrence of local minima of the objective function [32].

Figure 4 presents a system flow diagram showing the described calculation method.

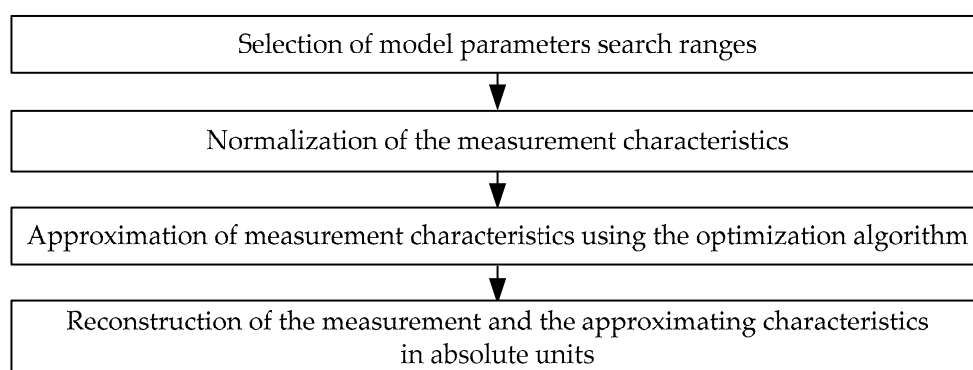


Figure 4. A system flow diagram showing the described calculation method.

As a quality measure of the reproduction of the supercapacitor studied by the selected mathematical model, the accuracy of the approximation of the frequency characteristics of the module and the argument of impedance was adopted. This accuracy should be the best in the widest possible frequency range. To compare the accuracy of the approximation of the characteristics for various supercapacitors with various models, the value of the objective function ε was used.

3. Results

The following symbols have been adopted in the tables and figures:

1. sym pp—symmetric supercapacitor with collectors containing polypyrrole;
2. Sym po—symmetric supercapacitor with collectors containing poly(3-n-octylpyrrole);
3. asym p_w—asymmetric supercapacitor, a working electrode connected to a collector containing polypyrrole;
4. asym o_w—asymmetric supercapacitor, a working electrode connected to a collector containing poly(3-n-octylpyrrole).

In order to approximate the morphological structure of the polymers, images were taken using a scanning electron microscope (SEM) instrument by Phenom ProX. SEM images were taken with 1000× zoom (Figures 5 and 6).

In Table 1, the results of the specific capacitance C_p of the supercapacitors tested are presented.

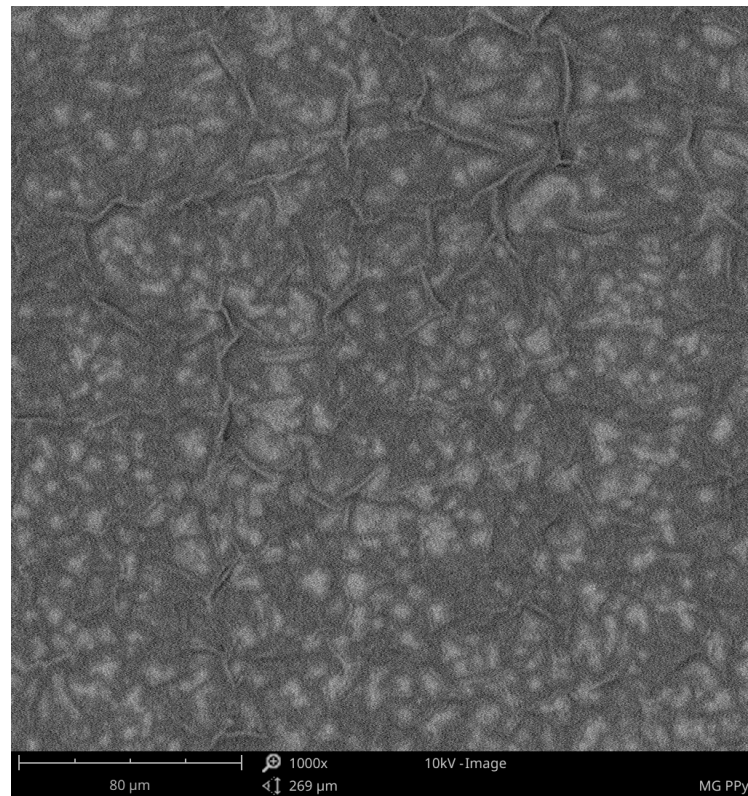


Figure 5. SEM photo of the polypyrrole, zoom $\times 1000$.

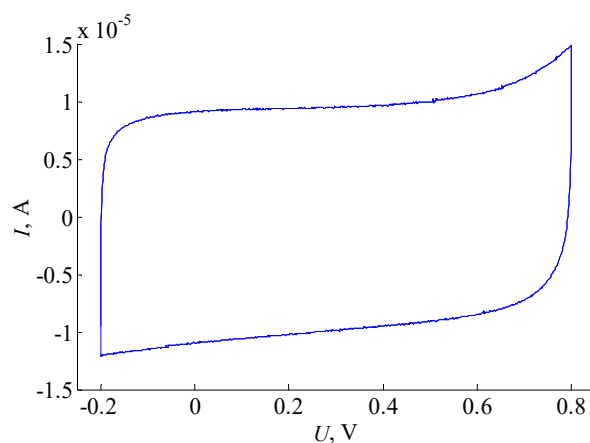


Figure 6. SEM photo of a poly(3-n-octylpyrrole), zoom $\times 1000$.

Table 1. The results of the specific capacitance C_p of the tested supercapacitors.

Type of supercapacitors	C_p , F/g
lithium perchlorate (LiClO₄)	
sym pp	49.04
sym po	10.23
asym p_w	23.80
asym o_w	23.65
tetrabutylammonium perchlorate (NBu₄ClO₄)	
sym pp	39.56
sym po	8.05
asym p_w	22.95
asym o_w	19.60
tetrabutylammonium triflate (NBu₄CF₃SO₃)	
sym pp	34.31
sym po	3.75
asym p_w	16.91
asym o_w	12.75
lithium trifluoromethanesulfonate (LiCF₃SO₃)	
sym pp	37.37
sym po	5.04
asym p_w	15.24
asym o_w	18.38

Figure 7 shows a cyclic voltammogram of the symmetric supercapacitor containing LiClO₄ as the active electrolyte component, with collectors containing polypyrrole.

**Figure 7.** Cyclic voltammogram of the symmetric supercapacitor containing LiClO₄ as the active electrolyte component, with collectors containing polypyrrole.

The research analyzed the accuracy of the approximation of the supercapacitor impedance frequency characteristics with the use of all models described in the article. Research results are presented for models that most accurately approximate the characteristics of the supercapacitors tested. The zero value of the offset voltage U (DC component of the voltage at the terminals of the tested supercapacitor) was assumed.

The frequency characteristics of the supercapacitor impedance differ depending on the active electrolyte component and the electrode material on each of the two collectors. In the case of asymmetric supercapacitors, these characteristics are also influenced by the way the electrodes are connected.

Figure 8 shows the impedance measurement characteristics of the tested supercapacitors with various active electrolyte components, for example, for symmetric supercapacitors with collectors containing polypyrrole.

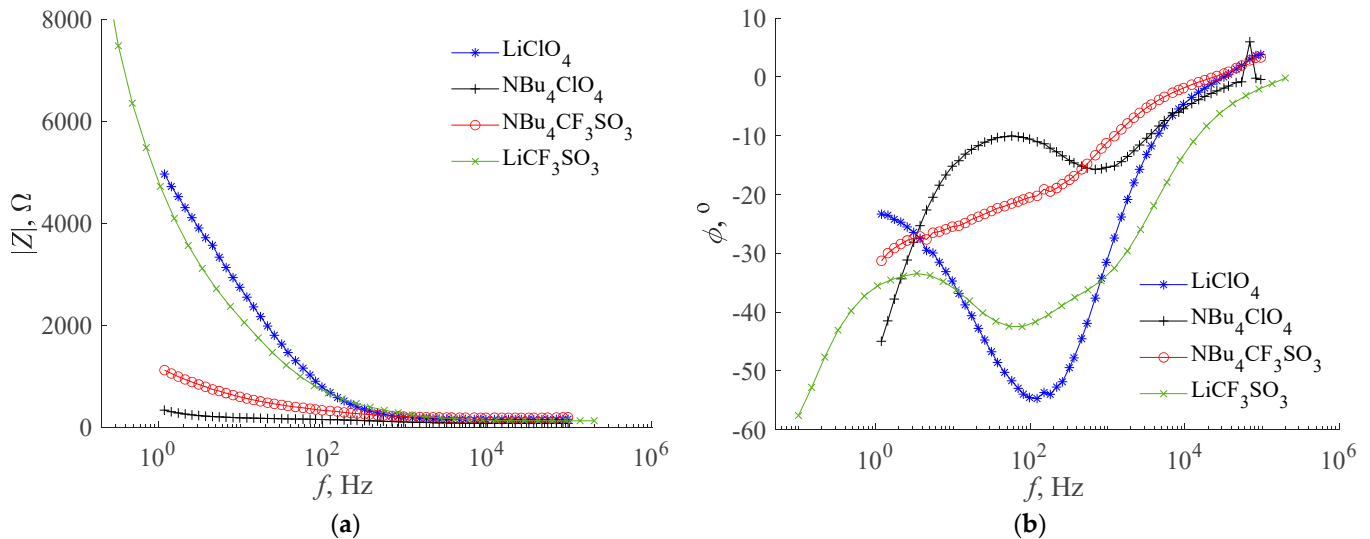


Figure 8. Measurement frequency characteristics of: (a) modulus and (b) argument of impedance of the tested symmetric supercapacitors with collectors containing polypyrrole.

Figure 9 shows the impedance measurement characteristics of the tested supercapacitors with different electrode materials on each of the two collectors, for example, for supercapacitors containing NBu_4ClO_4 as the active electrolyte component.

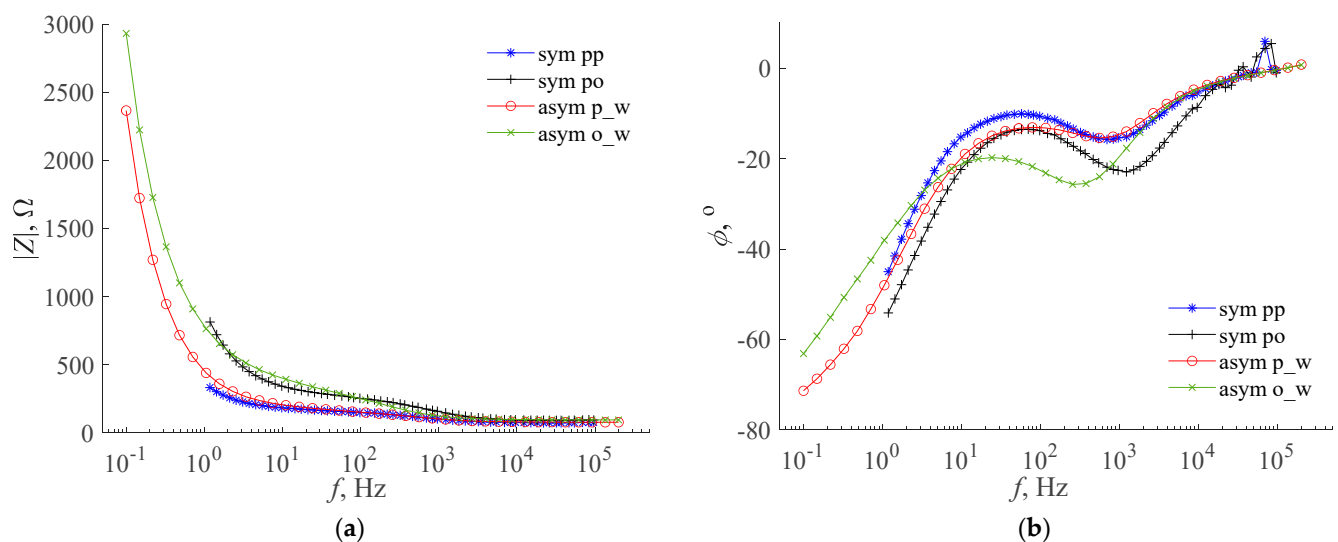


Figure 9. Measurement frequency characteristics of: (a) modulus and (b) argument of impedance of the tested symmetric supercapacitors containing NBu_4ClO_4 as the active electrolyte component.

Figure 10 shows the measurement and approximation characteristics, for example, for a symmetrical supercapacitor with collectors containing polypyrrole, containing LiClO_4 as the active electrolyte component.

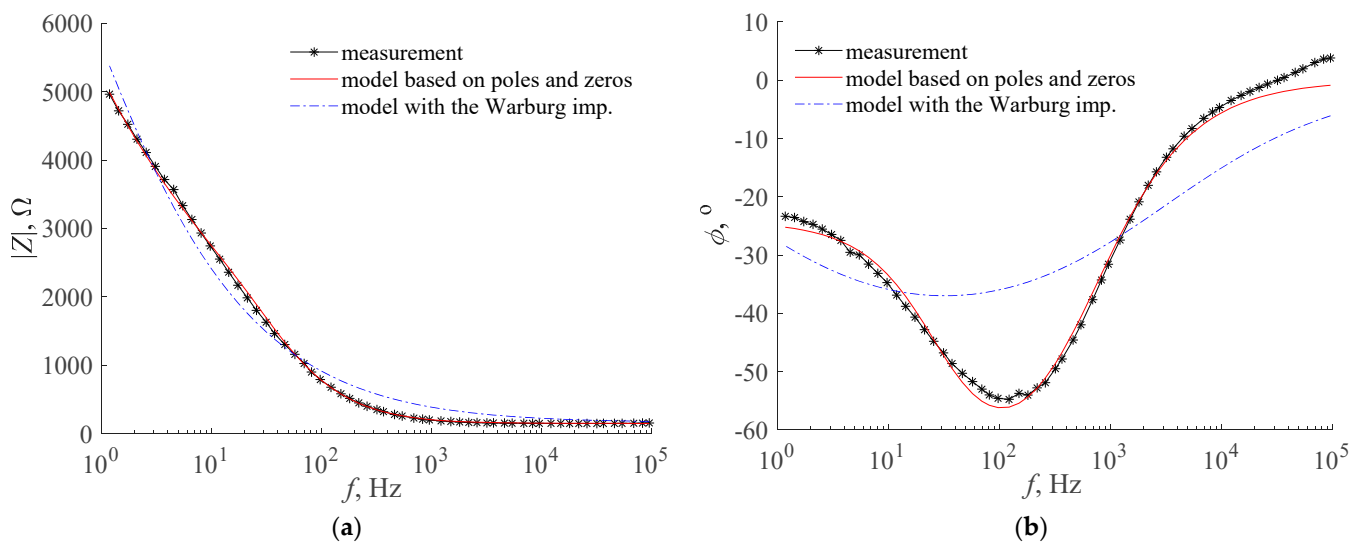


Figure 10. Measurement and approximating frequency characteristics of: (a) modulus and (b) argument of impedance of a symmetrical supercapacitor with collectors containing polypyrrole, containing LiClO_4 as an active electrolyte component.

In Tables 2 and 3, the results of the parameter estimation of the selected models, which showed the best fit in a wide frequency range and the mean square error value ε between the measurement and the approximating characteristics, are presented. Thanks to the normalization of the characteristics according to the formula (7), the error value ε can be used to compare the accuracy of the approximation of the characteristics for supercapacitors containing electrolytes with different active salts [32].

Table 2. Results of the estimation of the parameters of the model based on poles and zeros of the fractional-order impedance.

	k	ω_0	α	β	R_C	error ε
lithium perchlorate (LiClO_4)						
sym pp	8424.3	185.56	−0.56367	0.27405	146.85	0.058637
sym po	3828.4	259.3	−0.45725	0.33503	76.65	0.16693
asym p_w	1352.5	1347.4	−0.59429	0.29479	72.014	0.19888
asym o_w	1616.4	477.76	−0.56389	0.2352	62.64	0.061291
tetrabutylammonium perchlorate (NBu_4ClO_4)						
sym pp	1465.8	8.0341	0.70812	0.92687	56.177	0.40087
sym po	4031.3	10.966	0.62814	0.8955	70.833	0.61297
asym p_w	1609.4	9.8724	0.52107	0.80999	66.543	0.043923
asym o_w	2040.1	23691	−1.7018	0.4795	97.362	0.61096
tetrabutylammonium triflate ($\text{NBu}_4\text{CF}_3\text{SO}_3$)						
sym pp	2167.6	2440.5	−0.47945	0.39377	184.62	0.062268
sym po	3426.5	639.38	−0.45559	0.28419	110.46	0.15369
asym p_w	2120.2	8898.6	−0.7408	0.36878	117.53	0.35233
asym o_w	3299.4	349.14	−0.54399	0.25386	142.63	0.065157
lithium trifluoromethanesulfonate (LiCF_3SO_3)						
sym pp	11115	1237.4	−0.20086	0.45873	103.74	0.23864
sym po	2494.6	1370.9	−0.60748	0.34568	111.98	0.56962
asym p_w	1707.3	15.035	0.54098	0.81436	67.561	0.012915
asym o_w	1928.1	10.482	0.53368	0.81183	56.655	0.02344

Table 3. Results of the estimation of the parameters of the model with the Warburg limited impedance.

	C	R_1	R_2	Z_0	B	error ϵ
lithium perchlorate (LiClO ₄)						
sym pp	0.068338	13763	158.65	21198	70168	2.3005
sym po	0.11296	6441.9	73.134	7715.2	157040	1.7026
asym p_w	5.1356×10^{-4}	892.3	69.498	6289.3	23706	1.2981
asym o_w	0.0013897	1552.3	58.296	7293.1	67880	1.6432
tetrabutylammonium perchlorate (NBu ₄ ClO ₄)						
sym pp	5.8999×10^{-4}	216.53	100.34	8137.8	46950	0.16901
sym po	2.0493×10^{-4}	419.49	105.75	11843	118380	0.32735
asym p_w	6.6418×10^{-4}	424.6	104.02	2688.6	425780	0.14532
asym o_w	5.7118×10^{-4}	973.77	99.314	5219.9	477820	0.17531
tetrabutylammonium triflate (NBu ₄ CF ₃ SO ₃)						
sym pp	4.4654×10^{-4}	1494.3	196.09	5923.3	99632	0.21563
sym po	2.5466×10^{-4}	2527.3	104.72	13704	163990	1.1482
asym p_w	2.1319×10^{-4}	909.13	126.47	9495.3	68987	0.39841
asym o_w	0.0017873	3603.9	131.39	12135	149330	1.5139
lithium trifluoromethanesulfonate (LiCF ₃ SO ₃)						
sym pp	1.5192×10^{-4}	9991.4	116.73	18016	2054400	0.14238
sym po	1.9457×10^{-4}	1282.7	112.81	9213.3	131880	1.0919
asym p_w	6.8501×10^{-4}	839.92	115.35	1092.4	199870	0.098391
asym o_w	5.502×10^{-4}	448.69	92.663	3060.1	467300	0.15339

4. Discussion

Based on the research, the following conclusions were drawn:

- From the SEM analysis, we can know the local structure of polypyrrole and poly(3-n-octylpyrrole) surfaces. The polypyrrole surface is continuous and has three-dimensional structures that are evenly distributed over the surface. The surface of poly(3-n-octylpyrrole) has surface defects and uneven three-dimensional structures. For this reason, it can be assumed that the better electrochemical properties of polypyrrole result from its more ordered structure and the continuity of the polymer surface on the ITO plate;
- Among the polymers studied, polypyrrole turned out to be the best electrode material used as the electrode material. Supercapacitors containing this polymer covered ITO plates and an electrolyte containing lithium perchlorate (LiClO₄) showed the highest specific capacitance of 49 F/g (Table 1). The tested asymmetric supercapacitors have two different electrode materials: polypyrrole and poly(3-n-octylpyrrole). The values of the parameters tested in asymmetric supercapacitors, such as specific capacitance, turned out to be higher than the parameters obtained during the study of supercapacitors based on poly(3-n-octylpyrrole), but lower than those of systems containing polypyrrole;
- Figures 8 and 9 show that the type of active electrolyte component has the greatest influence on the shape of the frequency characteristic of the impedance modulus and argument. The effect of the electrode material is much smaller but also significant;
- The use of normalization of the measurement and approximation characteristics allows for the use of the error value ϵ to compare the approximation accuracy of the characteristics of different supercapacitors, although these characteristics have different ranges of values [32]. For example, Figure 10 shows that the accuracy of the approximation of the impedance argument of a symmetric supercapacitor with collectors containing polypyrrole, containing LiClO₄ as the active electrolyte component, is satisfactory for the model based on poles and zeros of fractional-order impedance, which corresponds to a small error value ϵ in Table 2. On the other hand,

the approximation accuracy of the impedance argument of this supercapacitor is not satisfactory for the model with the Warburg limited impedance, which corresponds to the large error value ε in Table 3;

- Among all optimization algorithms tested (including a hybrid algorithm [38–41], which is a combination of a genetic and a Newton gradient algorithm, used in the previous work of the author on evaluating the stability of the power system, including [42,43]), the best effectiveness and accuracy of the characteristic approximation were obtained for the Particle Swarm Optimization (PSO) algorithm [33–38]. The paper [38] presents a ranking of the effectiveness of various optimization algorithms used to analyze the optimal sizing of batteries in microgrids based on different features of the battery. The Ranker Search algorithm [38] ranks first, and the PSO algorithm ranks second. For our research, the Ranker Search algorithm is not a good solution, because it is looking for an optimal solution in a previously prepared data set. Creating such a data set would require the discretization of the value of the parameters sought. The PSO algorithm searches for the space of the objective function parameters in a continuous manner, without the need to create a discrete data set;
- For all supercapacitors and mathematical models tested, a satisfactory approximation accuracy of the impedance modulus characteristics was obtained. In each case, this accuracy was better than for the characteristics of the impedance argument. This regularity is also confirmed by the research conducted by the authors so far, among others described in [32];
- For most of the supercapacitors tested, the accuracy of the approximation of impedance characteristics was better for the model based on poles and zeros of the fractional-order impedance (3) than for the models with the Warburg impedance (4) and (5). This is especially noticeable with supercapacitors containing LiClO_4 as the active electrolyte component. In the studies described in [32], a similar regularity was also observed;
- For all cases, a very high value of parameter B of the model with limited Warburg impedance was obtained. Therefore, in formula (5), the value of the coth function is always close to 1 and this model can be reduced to the model with the Warburg impedance (4), while the values of the other parameters will not change. In the study, the parameters of the model (4) were also estimated and the obtained values of its parameters were very similar to the values of the parameters of the model (5) [32];
- The parameter k in the model based on poles and zeros of the fractional-order impedance is related to the reciprocal of the supercapacitor capacity. Based on the results from Table 2, it can be seen that in most cases the highest capacitance values and the smallest R_C resistance values were obtained for asymmetric supercapacitors. In each of the investigated cases of asymmetric supercapacitors, a higher capacity was obtained when the working electrode was connected to a polypyrrole-containing collector. The asymmetric supercapacitor, which contains LiClO_4 as the active electrolyte component, had the highest capacitance and relatively small R_C resistance;
- In the case of the model with limited Warburg impedance, on the basis of the results in Table 3, similar conclusions can be drawn. However, the analysis should not take into account results with large values of the ε error;
- In Table 4, a comparison has been made between the proposed approach of the optimization process and fractional-order model estimations presented in the paper, and the state-of-the-art solutions, mostly used in supercapacitors studies.

Table 4. Comparison between the state-of-the-art approach and the proposed optimization technique used in the paper.

Traditional Approach	Authors' Approach
The mechanism of storing electrical energy is based on an electrical double Helmholtz layer, which is formed at the interface between the electrolyte and the electrode [1,7,44].	The mechanism of storing electrical energy is faradaic and based on a double Helmholtz layer and the reduction and oxidation reactions of conductive polymers [10,14–16,44].
The parameters of supercapacitors (such as capacitance C and internal series resistance ESR) are determined based on charge and discharge waveforms by a constant current [18,19,45–47].	The parameters of supercapacitors have been estimated on the basis of the frequency characteristics obtained using the electrochemical impedance spectroscopy (EIS) method [19,21,22]. The parameters are of fractional order [24–27].
The series internal resistance ESR is usually determined by the voltage drop across a pre-charged supercapacitor over several tens of minutes [46–48].	The series internal resistance ESR has been defined as the impedance value for high-frequency values when the capacitive part of the impedance tends to zero, within the use of the Particle Swarm Optimization for the determination of the model parameters [20,32,48].

Author Contributions: Conceptualization, M.G., A.J.-C. and P.P.; methodology, P.P.; software, P.P.; validation, M.G., A.J.-C. and P.P.; formal analysis, P.P.; investigation, M.G.; resources, M.G.; data curation, M.G. and P.P.; writing—original draft preparation, M.G., A.J.-C. and P.P.; writing—review and editing, M.G., A.J.-C. and P.P.; visualization, P.P.; supervision, M.G., A.J.-C. and P.P.; project administration, M.G., A.J.-C. and P.P. All authors have read and agreed to the published version of the manuscript.

Funding: This research received no external funding.

Data Availability Statement: Not applicable.

Conflicts of Interest: The authors declare no conflict of interest.

References

- Subasinghage, K.; Gunawardane, K.; Padmawansa, N.; Kularatna, N.; Moradian, M. Modern Supercapacitors Technologies and Their Applicability in Mature Electrical Engineering Applications. *Energies* **2022**, *15*, 7752. [[CrossRef](#)]
- Gilev, B.; Andreev, M.; Hinov, N.; Angelov, G. Modeling and Simulation of a Low-Cost Fast Charging Station Based on a Micro Gas Turbine and a Supercapacitor. *Energies* **2022**, *15*, 8020. [[CrossRef](#)]
- Khodaparastan, M.; Mohamed, A. Supercapacitors for Electric Rail Transit Systems. In Proceedings of the 6th International Conference on Renewable Energy Research and Applications (ICRERA), San Diego, CA, USA, 5–8 November 2017; pp. 896–901. [[CrossRef](#)]
- Nguyen, T.H.; Nawaz, A.; Sreekumar, P.; Natsheh, A.; Akre, V.; Van, T.L. Implementation and Validation for Multitasks of a Cost-Effective Scheme Based on ESS and Braking Resistors in PMSG Wind Turbine Systems. *Energies* **2022**, *15*, 8282. [[CrossRef](#)]
- Jamal, S.; Pasupuleti, J.; Rahmat, N.A.; Tan, N.M.L. Energy Management System for Grid-Connected Nanogrid during COVID-19. *Energies* **2022**, *15*, 7689. [[CrossRef](#)]
- Wang, B.; Wang, C.; Wang, Z.; Ni, S.; Yang, Y.; Tian, P. Adaptive state of energy evaluation for supercapacitor in emergency power system of more-electric aircraft. *Energy* **2023**, *263*, 125632. [[CrossRef](#)]
- Geng, Z.; Mannerhagen, F.; Thiringer, T. *Characterization of Lithium Ion Supercapacitors*; Institute of Electrical and Electronics Engineers: Piscataway, NJ, USA, 2020; ISBN 978-9-0758-1536-8. [[CrossRef](#)]
- Pullanchiyodan, A.; Manjakkal, L.; Dahiya, R. Metal Coated Fabric Based Asymmetric Supercapacitor for Wearable Applications. *IEEE Sens. J.* **2021**, *21*, 26208–26214. [[CrossRef](#)]
- Bogusz, W.; Krok, F. *Solid Electrolytes, Electrical Properties and Methods of Their Measurement*, Wyd; Naukowo-Techniczne: Warszawa, Poland, 1995. (In Polish)
- Gocki, M. Research on the Application of Selected Conductive Polymers for Electricity Storage. Master's Thesis, Department of Physicochemistry and Polymer Technology, Faculty of Chemistry, Silesian University of Technology, Gliwice, Poland, 2021. (In Polish)
- Song, Y.; Shang, M.; Li, J.; Su, Y. Continuous and controllable synthesis of MnO₂/PPy composites with core-shell structures for supercapacitors. *Chem. Eng. J.* **2020**, *405*, 127059. [[CrossRef](#)]

12. Tong, L.; Jiang, C.; Cai, K.; Wei, P. High-performance and freestanding PPy/Ti3C2Tx composite film for flexible all-solid-state supercapacitors. *J. Power Sources* **2020**, *465*, 228267. [[CrossRef](#)]
13. Wen, J.; Xu, B.; Zhou, J.; Chen, Y. Novel high-performance asymmetric supercapacitors based on nickel-cobalt composite and PPy for flexible and wearable energy storage. *J. Power Sources* **2018**, *402*, 91–98. [[CrossRef](#)]
14. Krajewska, A. Development of Electrochemical Sensors for the Determination of Acrylamide and Acrylic Acid in Food Products. Ph.D. Dissertation, Faculty of Chemistry, Gdańsk University of Technology, Gdańsk, Poland, 2009. (In Polish).
15. Geiger, W.E.; Barričre, F. Organometallic Electrochemistry Based on Electrolytes Containing Weakly-Coordinating Fluoroarylborate Anions. *Accounts Chem. Res.* **2010**, *43*, 1030–1039. [[CrossRef](#)]
16. Lisowska-Oleksiak, A.; Nowak, A.P.; Wilamowska, M. Supercapacitors as Energy Storage Materials. *Acta Energetica* **2015**, *7*, 71–78. (In Polish)
17. Filip, A.; Musat, V.; Tigau, N.; Polosan, S.; Pimentel, A.; Ferreira, S.; Gomes, D.; Calmeiro, T.; Martins, R.; Fortunato, E. ZnO nanostructures grown on ITO coated glass substrate by hybrid microwave-assisted hydrothermal method. *Optik* **2020**, *208*, 164372. [[CrossRef](#)]
18. Gualous, H.; Bouquain, D.; Berthon, A.; Kauffmann, J. Experimental study of supercapacitor serial resistance and capacitance variations with temperature. *J. Power Sources* **2003**, *123*, 86–93. [[CrossRef](#)]
19. Helseth, L. Comparison of methods for finding the capacitance of a supercapacitor. *J. Energy Storage* **2021**, *35*, 102304. [[CrossRef](#)]
20. Gocki, M.; Nowak, A.J. Analysis of the Characteristics of Electrically Conductive Polymers Using the Electrochemical Impedance Spectroscopy Method. In *International Student Scientific Conference TalentDetector2022_Winter, Works of the Depart. of Eng. and Bio. Mat.*; Silesian University of Technology: Gliwice, Poland, 2022; pp. 231–238. (In Polish)
21. Buller, S.; Karden, E.; Kok, D.; De Doncker, R. Modeling the dynamic behavior of supercapacitors using impedance spectroscopy. *IEEE Trans. Ind. Appl.* **2002**, *38*, 1622–1626. [[CrossRef](#)]
22. Freeborn, T.J.; Maundy, B.; Elwakil, A.S. Fractional-order models of supercapacitors, batteries and fuel cells: A survey. *Mater. Renew. Sustain. Energy* **2015**, *4*, 1–7. [[CrossRef](#)]
23. Omori, T.; Nakanishi, M.; Tashima, D. Modeling of Equivalent Circuit Analysis of Degraded Electric Double-Layer Capacitors. *Materials* **2021**, *14*, 435. [[CrossRef](#)] [[PubMed](#)]
24. Martín, R.; Quintana, J.J.; Ramos, A.; de la Nuez, I. Modeling electrochemical double layer capacitor, from classical to fractional impedance. In *Proceedings of the 14th Mediterranean Electrotechnical Conference, Ajaccio, France, 5–7 May 2008*; pp. 61–66. [[CrossRef](#)]
25. Martín, R.; Quinatana, J.; Ramos, A.; Nuez, I.; Martín, A.R. Fractional equivalent impedance of electrochemical double layer capacitors combinations. *J. Eur. Des. Syst. Autom.* **2008**, *42*, 923–928. [[CrossRef](#)]
26. Martín, A.R.; Quintana, J.J.; Ramos, A.; De La Nuez, I. Modeling of Electrochemical Double Layer Capacitors by Means of Fractional Impedance. *J. Comput. Nonlinear Dyn.* **2008**, *3*, 61–66. [[CrossRef](#)]
27. Hidalgo-Reyes, J.; Gómez-Aguilar, J.; Jiménez, R.E.; Alvarado-Martinez, V.; Lopez-Lopez, M. Determination of supercapacitor parameters based on fractional differential equations. *Int. J. Circuit Theory Appl.* **2019**, *47*, 1225–1253. [[CrossRef](#)]
28. Czerwiński, W.; Kaczmarek, H.; Kędziera, D. *Conductive and Photosensitive Polymer Materials*; Nicolaus Copernicus University: Toruń, Poland, 2012.
29. Kwon, H.; Han, D.J.; Lee, B.Y. All-solid-state flexible supercapacitor based on nanotube-reinforced polypyrrole hollowed structures. *RSC Adv.* **2020**, *10*, 41495–41502. [[CrossRef](#)] [[PubMed](#)]
30. Semary, M.S.; Fouda, M.E.; Hassan, H.; Radwan, A.G. Realization of fractional-order capacitor based on passive symmetric network. *J. Adv. Res.* **2019**, *18*, 147–159. [[CrossRef](#)] [[PubMed](#)]
31. Jakubowska-Ciszek, A.; Walczak, J. Frequency Method for Determining the Equivalent Parameters of Fractional-Order Elements $L_{\beta}C_{\alpha}$. In *Proceedings of the Conference on Non-Integer Order Calculus and Its Applications RRNR 2018, Białystok, Poland, 20–21 September 2018*; Springer Nature: Berlin/Heidelberg, Germany, 2018; pp. 250–267. [[CrossRef](#)]
32. Gocki, M.; Jakubowska-Ciszek, A.; Pruski, P. Measurement Estimation of the Fractional-Order Models Parameters of a New Class of Symmetrical Polymer Supercapacitors. *Przegląd Elektrotechniczny* **2022**, *11*, 224–228. (In Polish) [[CrossRef](#)]
33. Poli, R.; Kennedy, J.; Blackwell, T. Particle Swarm Optimization. An Overview. *Swarm Intell.* **2007**, *1*, 33–57. [[CrossRef](#)]
34. Fernandes, C.M.; Rosa, A.C.; Fachada, N.; Laredo, J.L.J.; Merelo, J.J. Particle Swarm and Population Structure. In *Proceedings of the Genetic and Evolutionary Computation, Conference Companion GECCO, Kyoto, Japan, 15–19 July 2018*; pp. 85–86. [[CrossRef](#)]
35. Cleghorn, C.W.; Engelbrecht, A.P. Fitness-Distance-Ratio Particle Swarm Optimization: Stability Analysis. In *Proceedings of the Genetic and Evolutionary Computation, Conference Companion GECCO, Kyoto, Japan, 15–19 July 2018*; pp. 12–18. [[CrossRef](#)]
36. Fan, Y.; An, H.; Zhao, R. Double Traction Strategy Particle Swarm Optimization Algorithm. In *Proceedings of the International Conference on Computers, Information Processing and Advanced Education CIPAE, Ottawa, ON, Canada, 16–18 October 2020*; pp. 206–210. [[CrossRef](#)]
37. Li, W.; Fan, Y.; Jiang, Q.; Xu, Q. Velocity-Driven Particle Swarm Optimization. In *Proceedings of the 8th International Conference on Computing and Pattern Recognition ICCPR, Beijing, China, 23–25 October 2019*; pp. 9–16. [[CrossRef](#)]
38. Khan, H.; Nizami, I.F.; Qaisar, S.M.; Waqar, A.; Krichen, M.; Almaktoom, A.T. Analyzing Optimal Battery Sizing in Microgrids Based on the Feature Selection and Machine Learning Approaches. *Energies* **2022**, *15*, 7865. [[CrossRef](#)]
39. Khanh, D.V.; Vasant, P.; Elamvazuthi, I.; Dieu, V.N. Optimization Of Thermo-Electric Coolers Using Hybrid Genetic Algorithm And Simulated Annealing. *Arch. Control Sci.* **2014**, *24*, 155–176. [[CrossRef](#)]

40. Paszek, S.; Nocoń, A. *Optimisation and Polyoptimisation of Power System Stabilizer Parameters*; LAMBERT Academic Publishing: Saarbrücken, Germany, 2014.
41. Wörner, L.; Kulig, S.; Willing, M.; Winzer, P. Genetic Algorithm Embedded into a Quality-Oriented Workflow of Methods for the Development of a Linear Drive used in Intralogistic Systems. *Arch. Electr. Eng.* **2014**, *63*, 647–665. [[CrossRef](#)]
42. Pruski, P.; Paszek, S. Location of generating units most affecting the angular stability of the power system based on the analysis of instantaneous power waveforms. *Arch. Control Sci.* **2020**, *30*, 273–293. [[CrossRef](#)]
43. Pruski, P.; Paszek, S. Calculations of power system electromechanical eigenvalues based on analysis of instantaneous power waveforms at different disturbances. *Appl. Math. Comput.* **2018**, *319*, 104–114. [[CrossRef](#)]
44. Pershaanaa, M.; Bashir, S.; Ramesh, S.; Ramesh, K. Every bite of Supercap: A brief review on construction and enhancement of supercapacitor. *J. Energy Storage* **2022**, *50*, 104599. [[CrossRef](#)]
45. Gómez, F.; Rosales, J.; Guía, M. RLC electrical circuit of non-integer order. *Open Phys.* **2013**, *11*, 1361–1365. [[CrossRef](#)]
46. Burke, A. Ultracapacitors: Why, how, and where is the technology. *J. Power Sources* **2000**, *91*, 37–50. [[CrossRef](#)]
47. Freeborn, T.J.; Maundy, B.; Elwakil, A.S. Measurement of Supercapacitor Fractional-Order Model Parameters From Voltage-Excited Step Response. *IEEE J. Emerg. Sel. Top. Circuits Syst.* **2013**, *3*, 367–376. [[CrossRef](#)]
48. Vicentini, R.; Da Silva, L.M.; Cecilio Junior, E.P.; Alves, T.A.; Nunes, W.G.; Zanin, H. How to Measure and Calculate Equivalent Series Resistance of Electric Double-Layer Capacitors. *Molecules* **2019**, *24*, 1452. [[CrossRef](#)] [[PubMed](#)]

Disclaimer/Publisher’s Note: The statements, opinions and data contained in all publications are solely those of the individual author(s) and contributor(s) and not of MDPI and/or the editor(s). MDPI and/or the editor(s) disclaim responsibility for any injury to people or property resulting from any ideas, methods, instructions or products referred to in the content.